Distributed Power Management of Off-grid DC Fast Charging Station Integrated with Multi-microgrid System Under Uncertainty and Outage Conditions

Hossien Faraji, Amir Khorsandi, and Seyed Hossein Hosseinian

***Abstract*—Numerous studies nowadays have examined direct current fast charging (DCFC) stations equipped with distributed generations and storage devices or integrated with microgrid (MG) systems. However, none have proposed effective power management for off-grid DCFC stations integrated with multi-microgrid (MMG) system. In this paper, innovative distributed power management schemes (DPMSs) for off-grid DCFC station integrated with MMG system (DCFC-MMG) under uncertainty and outage conditions are proposed using distributed control systems (DCSs). The DCFC station is equipped with a central battery unit (CBU) and four charging locations (CLs). The MMG comprises three renewable MGs, which can meet their own energy demands of the power grid independently and provide fast charging for electric vehicles (EVs). Communication among MGs, CLs, and the CBU occurs through distributed interactions. Moreover, the MGs not only provide proper support from DCFC stations during CBU outage considering generation uncertainty and demand fluctuations, but also mutually support each other through microgrid-to-microgrid (MG2MG) interactions under critical conditions such as the outage of any MG batteries. Vehicle-to-vehicle (V2V) and vehicle-to-microgrid (V2MG) capabilities have also been designed to address situations where the MG batteries are simultaneously disconnected. Nonlinear time-domain simulation performed in the MATLAB/Simulink environment demonstrates that the proposed DPMSs for off-grid DCFC-MMG perform effectively under various uncertainty and outage conditions.**

***Index Terms*—Distributed power management, electric vehicle (EV), multi-microgrid, charging station (CS), uncertainty, outage.**

I. Introduction

THE widespread adoption of electric vehicles (EVs) relies heavily on the availability of direct current fast charging (DCFC) solutions [1]. Currently, these charging stations (CSs) primarily draw power from the grid, which can lead to increased demand during peak hours [2]. Additionally, the large-scale integration of CSs into the grid may cause issues such as excessive load density and voltage sags in distribution networks (DNs) [3]. In cases where the grid is unavailable, renewable energy sources (RESs) can serve as the main power supply for DCFC stations [4]. Another approach is to integrate DCFC stations with microgrids (MGs), which can enhance reliability and provide various ancillary services through their energy storage systems (ESSs) [5], and consequently enable economical and effective DCFC solutions for EVs [6]. This approach offers several advantages including reduced carbon emissions, lower electricity costs, and a more reliable power supply during grid outages [7].

Reference [8] introduces an effective multi-level charging system that enables EVs to specify their charging demands and obtain the most suitable charging rate. Multiple charging levels are featured within a single charger, with each level offering a different charging rate. In [9], a two-level structure for coordinated charging at a CS is proposed, prioritizing demand-based charging to improve the EV user's experience. In [10], a robust predictive control method is employed for the energy management of a smart CS with photovoltaic (PV) unit and ESS. The impact of CS on the grid is noted in [11], which identifies grid instability during fast charging. To address this, researchers suggest integrating MGs with RESs. Reference [12] explores the energy management of CSs with ESSs in a grid-connected mode, proposing a centralized model for physical constraints and a distributed coordination mechanism for decentralized implementation. The purpose of [13] is to explore how the integration of CS affects the optimal performance of MG-based supply infrastructure and its interaction with the DN. Reference [14] examines the reliable cooperative performance of MGs that include ESSs at CSs. A robust energy management system is first developed, and then, a robust optimization algorithm is designed. In [15], a controller for CS is proposed that allows the charger to support the connection voltage and damp transients without affecting the charging efficiency. In [16], the concept of charging capacity market is introduced, enabling the allocation and trading of charging capacity for CSs on a day-ahead basis. Unlike traditional day-ahead electricity markets, [16] addresses the uncertainty of EVs and ensures se-

Manuscript received: July 19, 2025; revised: October 28, 2025; accepted: February 26, 2026. Date of CrossCheck: February 26, 2026. Date of online publication: April 17, 2026.

H. Faraji, A. Khorsandi (corresponding author), and S. H. Hosseinian are with the Department of Electrical Engineering, Amirkabir University of Technology, Tehran, Iran (e-mail: hossien.faraji@aut.ac.ir; a_khorsandi@aut.ac.ir; hosseinian@aut.ac.ir).

DOI: 10.35833/MPCE.2025.000660

cure grid operations. In [17], a distributed control is proposed to send excess reactive power from CSs and distributed generations to normalize the voltage of DN without conventional voltage control devices such as on-load tap changers. In [18], to address the voltage profile imbalance issue affected by the presence of CS in the DN, a suitable integrated PV system is utilized considering environmental challenges. Reference [19] aims to develop an adaptive CS that employs RESs in an MG without imposing significant stress on the DN. Reference [20] presents a decentralized power management scheme for an off-grid CS powered by ESSs. This system features the integration of additional ESSs and RESs while reducing the system complexity. Furthermore, in [21], the financial benefits from using an EV battery as a temporary ESS in an MG integrated with PV units are investigated. In [22], a robust distributed energy management model for multi-microgrids (MMGs) including EVs is proposed, where uncertainties in RESs, loads, and EV communications are considered. In [23], an integrated control system for DCFC stations is introduced, effectively addressing the voltage sag issues and ensuring an optimal off-grid operation. Reference [24] discusses energy management in an MG that includes PV units, a wind turbine, an ESS, an EV, and a DC load, all connected to a DC bus and linked to an alternating current (AC) grid via a DC-AC converter, with the main goal of regulating the DC bus voltage. Reference [25] proposes a power management strategy for a DCFC station, aiming to maintain fast and reliable EV charging while reducing the dependence on grid. It introduces an improved optimal control method to enhance the performance of the grid-connected voltage source converter (VSC). In [26], a PV system combined with ESSs and a wind-driven islanded MG system is developed to provide continuous power to remote CSs. In [27], a pioneering framework for a wind-powered CS is introduced, employing an improved decentralized model-based predictive control to meet the charging demands of EVs with different control patterns. In [28], a multi-objective energy planning strategy for an off-grid MG focuses on the optimal management of its limited energy supply using an incentive-based demand response scheme. A point estimation method is used to address the uncertainty of EVs. Reference [29] is driven by the need to accelerate the adoption of EVs through decentralized and renewable energy-based CSs that are independent of the grid. The system in [29] consists of eight CSs and uses RESs to reduce grid dependency. Reference [30] conducts a techno-economic assessment of an off-grid PV-wind-hydrogen storage-based CS to determine the optimal configuration that meets the load demand.

As reviewed, various studies have aimed to improve the performance of CSs and reduce the load on DNs using diverse solutions. Several studies have optimized the charging process or provided multi-level coordinated charging, while others have equipped CSs with centralized or distributed storages. Additional studies have focused on integrating CSs with MGs, employing multifunctional energy management systems. However, none have addressed an off-grid DCFC station integrated with MMG system (DCFC-MMG) considering generation uncertainty, potential ESS outage, MMG support from the DCFC station, vehicle-to-microgrid (V2MG) capability, mutual support among MGs through microgrid-to-microgrid (MG2MG) facility, and EVs through vehicle-to-vehicle (V2V) capability in critical situations.

In this paper, distributed power management schemes (DPMSs) of off-grid DCFC-MMG using distributed control systems (DCSs) are presented. Three MGs, each equipped with a PV unit and an ESS, constitute the main structure of the MMG. The DCFC station is equipped with a central battery unit (CBU) and four charging locations (CLs). Under normal conditions, MGs 1-3 are used to charge CLs 1-3, respectively, in addition to supplying their internal three-phase loads. The CBU is responsible for CL 4. When the CBU is out of the circuit, MGs 1-3 operate cooperatively to supply CL 4, considering generation uncertainty. The CBU charging process is also carried out by the MGs during periods when the CLs are unoccupied. Furthermore, if one MG experiences a battery outage, the other two MGs support it. Also, by implementing V2V and V2MG capabilities, the CLs, with the assistance of the CBU, can meet the requirements of off-grid DCFC-MMG in critical situations where the MG batteries simultaneously fail. The major innovations of this paper are summarized as follows.

1) An off-grid DCFC-MMG is designed, modeled, and implemented using DCSs.

2) Applicable DPMSs are proposed by establishing appropriate interaction among MGs, CLs, and the CBU to provide mutual support among MGs in critical situations considering DCFC station requirements, and to handle simultaneous MG battery outages by implementing the V2V and V2MG capabilities.

3) The DCFC of EVs is enabled by an MMG without grid assistance under uncertainty and outage conditions.

4) The capability of MGs within the MMG is demonstrated to operate independently, interconnected with each other, and connected to the DCFC station without the presence of grid.

II. OFF-GRID DCFC-MMG

The diagram of an off-grid DCFC-MMG under study is shown in Fig. 1. Three MGs are connected to the DCFC station through three AC-DC converters (VSCs 1-3). The MGs are interconnected through three bidirectional DC-DC converters (BCs 1-3). Accordingly, the MGs can support both the DCFC station and each other.

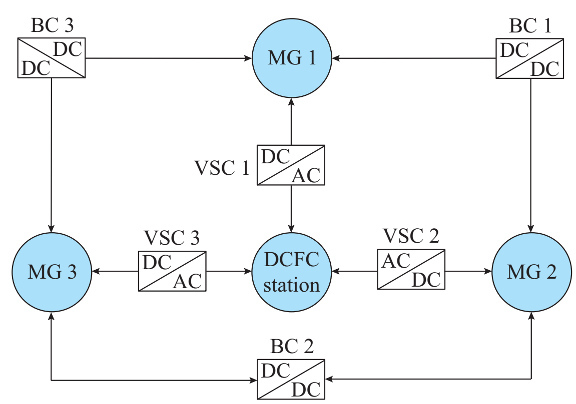

Fig. 1. Diagram of off-grid DCFC-MMG under study.

Further details of inner equipment used in off-grid DCFC-MMG are illustrated in Fig. 2. The DCFC station is equipped with a CBU and four CLs. The CLs and CBU are interfaced with the AC bus through AC-DC and DC-DC converters. Each CL is responsible for providing charging power to each of the EVs parked at the CLs, with a charging requirement of 150 kW at 620 V. If required, each CL can also operate in discharging mode with the same electrical characteristics. The CBU is similarly capable of bidirectional power exchange with the AC bus. In each MG, a three-phase inverter is responsible for supplying time-varying three-phase loads rated at 440 V/60 Hz. In addition, a PV unit and a battery are connected to a 660 V DC bus through boost and buck-boost converters, respectively. It is worth noting that all EV batteries are 400 V/80 kWh lithium-ion units. Table I summarizes the electrical specifications of the system components.

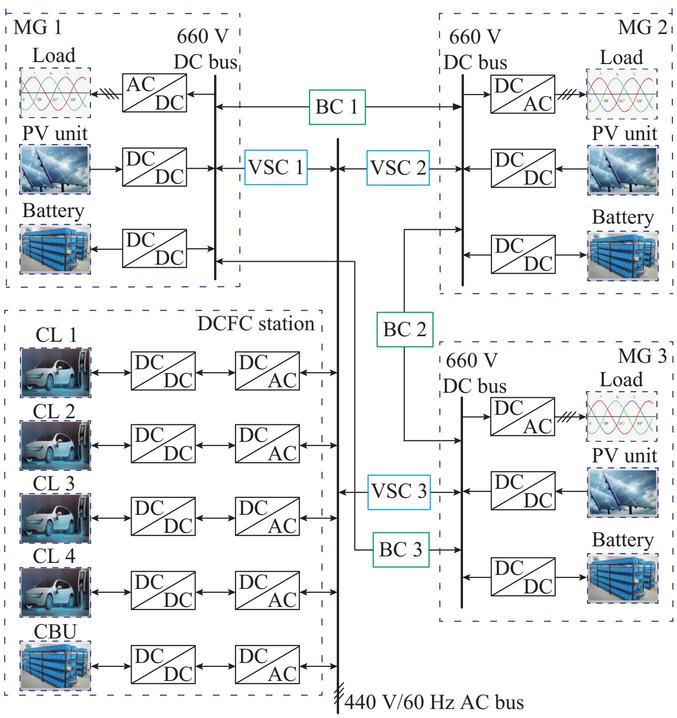

Fig. 2. Further details of inner equipment used in off-grid DCFC-MMG.

TABLE I
ELECTRICAL SPECIFICATIONS OF SYSTEM COMPONENTS

Component	Power or capacity	Voltage (V)
PV unit in MG	200 kW	400
PV converter in MG	250 kW	660
Battery in MG	650 Ah	600
Battery converter in MG	450 kW	660
DC-AC load inverter in MG	350 kVA	440
AC-DC converter in CL	200 kVA	440
DC-DC converter in CL	200 kW	620
Battery in CBU	500 Ah	800
AC-DC converter in CBU	400 kVA	660
DC-DC converter in CBU	400 kW	840
DC-DC converter in BC	300 kW	660
AC-DC VSC	300 kVA	440

III. PROPOSED DPMSs

A. Considerations of Generation Uncertainty and CBU Outage

To implement the proposed DPMSs, when the CBU is in the circuit, MGs 1-3 supply the required power for charging EVs 1-3 parked at CLs 1-3, respectively. The power injected from MGs 1-3 into the CLs is managed through VSCs 1-3, respectively, using the corresponding DCSs. In other words, there exists a communication link among the DCS of MG i, the DCS of VSC i, and the DCS of CL i, where $i=1, 2, 3$. Meanwhile, through the connection between the DCS of CL 4 and the DCS of CBU, the power required to charge EV 4 parked at CL 4 is supplied by the CBU.

If the CBU goes out of the circuit, MGs 1-3 jointly provide the required charging power for CL 4 through communication between the DCS of VSCs/MGs 1-3 and the DCS of CL 4, provided that the PV power generation of each MG is no less than 0.3 p.u.. In other words, an MG experiencing generation deficiency does not participate in the charging process of EV 4 in the absence of the CBU.

When the charging processes of EVs 1-3 are completed, MGs 1-3 do not lead to power injection, but instead inject power equal to half of the charging power (i.e., 75 kW) into the CBU. However, any MG with PV power generation less than 0.3 p.u. does not contribute to the CBU charging process. Figure 3 illustrates the flowchart of the proposed DPMSs for off-grid DCFC-MMG.

It is worth noting that the AC bus in the DCFC station acts as a common bus, and all three MGs are connected to this bus through the VSCs. Consequently, power flow within this bus follows circuit laws. Therefore, the assumption that MGs 1-3 charge EVs 1-3, respectively, acts only as a control allocation method. The reason for selecting the threshold of 0.3 p.u. is provided in Supplementary Material A.

Figure 4 displays the DCS for implementing the proposed DPMSs on off-grid DCFC-MMG based on the flowchart presented in Fig. 3. The equivalent impedance Z, including the resistance R and reactance X of each MG, CL, and the CBU connected to the AC bus is calculated in (1). Furthermore, the dynamic equations of each AC-DC converter considering the DC link voltage and switching effects are obtained from (2).

$$Z_i = R_i + X_i \tag{1}$$

$$\begin{cases} \dfrac{\mathrm{d}I_\mathrm{a}}{\mathrm{d}t} = -\dfrac{R}{Z}I_\mathrm{a} - \dfrac{1}{Z}V_\mathrm{a} + \dfrac{V_{dc}}{3L}(2K_\mathrm{a} - K_\mathrm{b} - K_\mathrm{c}) \\ \dfrac{\mathrm{d}I_\mathrm{b}}{\mathrm{d}t} = -\dfrac{R}{Z}I_\mathrm{b} - \dfrac{1}{Z}V_\mathrm{b} + \dfrac{V_{dc}}{3L}(-K_\mathrm{a} + 2K_\mathrm{b} - K_\mathrm{c}) \\ \dfrac{\mathrm{d}I_\mathrm{c}}{\mathrm{d}t} = -\dfrac{R}{Z}I_\mathrm{c} - \dfrac{1}{Z}V_\mathrm{c} + \dfrac{V_{dc}}{3L}(-K_\mathrm{a} - K_\mathrm{b} + 2K_\mathrm{c}) \end{cases} \tag{2}$$

where V and I are the voltages and currents in the three-phase domain, respectively; L is the line inductance; V_{dc} is the DC bus voltage; K is the coefficient that can take values of 0 or 1 depending on the state of the upper and lower switches of hysteresis current controller (HCC) [31]; and subscripts a, b, and c denote the three phases.

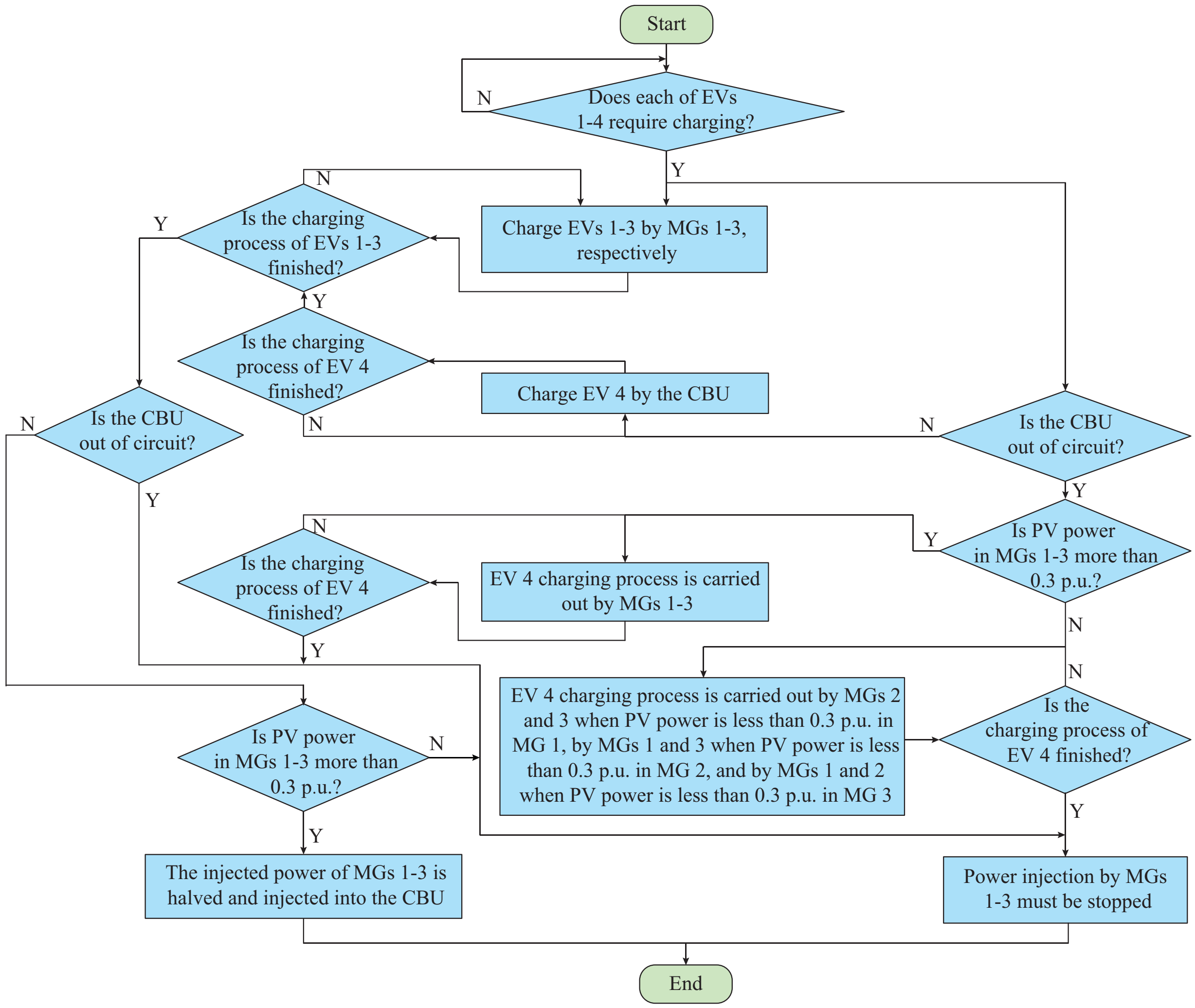

Fig. 3. Flowchart of proposed DPMSs for off-grid DCFC-MMG.

It is worth noting that in Fig. 4, the indices *ref* and *reg* denote the reference and regulated values, respectively; subscripts d and q denote the d- and q-axis components, repectively; ω is the angular speed; P is the active power of AC-DC converters associated with the CLs, MGs, and the CBU in the d-q frame; *VSC*, *CL*, *CBU*, and *EV* in the subscripts or superscripts denote the corresponding VSC, CL, CBU, and EV, respectively; the variables with "*" denote the decoupled terms; *R*&*X* denotes the impedance; SOC denotes the state of charge; PI denotes proportional-integral; and PWM denotes the pulse width modulation.

$$\boldsymbol{T}_{dq}^{\text{abc}}=\frac{2}{3}\begin{bmatrix}\cos(\omega t) & \cos(\omega t-2\pi/3) & \cos(\omega t+2\pi/3)\\ -\sin(\omega t) & -\sin(\omega t-2\pi/3) & -\sin(\omega t+2\pi/3)\end{bmatrix} \tag{3}$$

$$\begin{cases}\dfrac{\mathrm{d}I_d}{\mathrm{d}t}=-\dfrac{R}{Z}I_d+\dfrac{K_d}{Z}V_{dc}-\dfrac{1}{Z}V_d+\omega I_q\\ \dfrac{\mathrm{d}I_q}{\mathrm{d}t}=-\dfrac{R}{Z}I_q+\dfrac{K_q}{Z}V_{dc}-\dfrac{1}{Z}V_q-\omega I_d\end{cases} \tag{4}$$

$$\begin{cases}V_d^*=-\omega I_q\\ V_q^*=\omega I_d\end{cases} \tag{5}$$

$$P=3(V_dI_d+V_qI_q)/2 \tag{6}$$

where $\boldsymbol{T}_{dq}^{\text{abc}}$ is the transfer matrix from the three-phase domain to the d-q frame. The process described in (3) transfers the dynamic model acquired in (2) from the three-phase domain to the d-q frame. Consequently, the d-q current equations are derived in (4). By incorporating the coefficients in (5) to (4), independent control of the d-q currents is enabled. After the d-q currents are calculated, the active power P is calculated in (6). As shown in Fig. 4, the control along the d-axis is considered to represent the active power exchange, and the control along the q-axis corresponding to reactive power exchange among subsystems is not considered.

For triggering the AC-DC converters in each MG, CL, and CBU, the active power calculated in (6) is compared with the reference power value determined by the corresponding DCS to calculate the reference current of the d-axis. Then, by comparing this current with the DC reference current, the regulated current of the d-axis is obtained. PI controllers are employed for these control loops. The calculated currents are then transformed from the d-q frame to three-phase domain by matrix $\boldsymbol{T}_{\text{abc}}^{dq}$ in (7). Finally, these currents are compared with the output currents of AC-DC converters in the three-phase domain as per (8) to generate the appropriate gating pulses for the AC-DC converters by the HCC units.

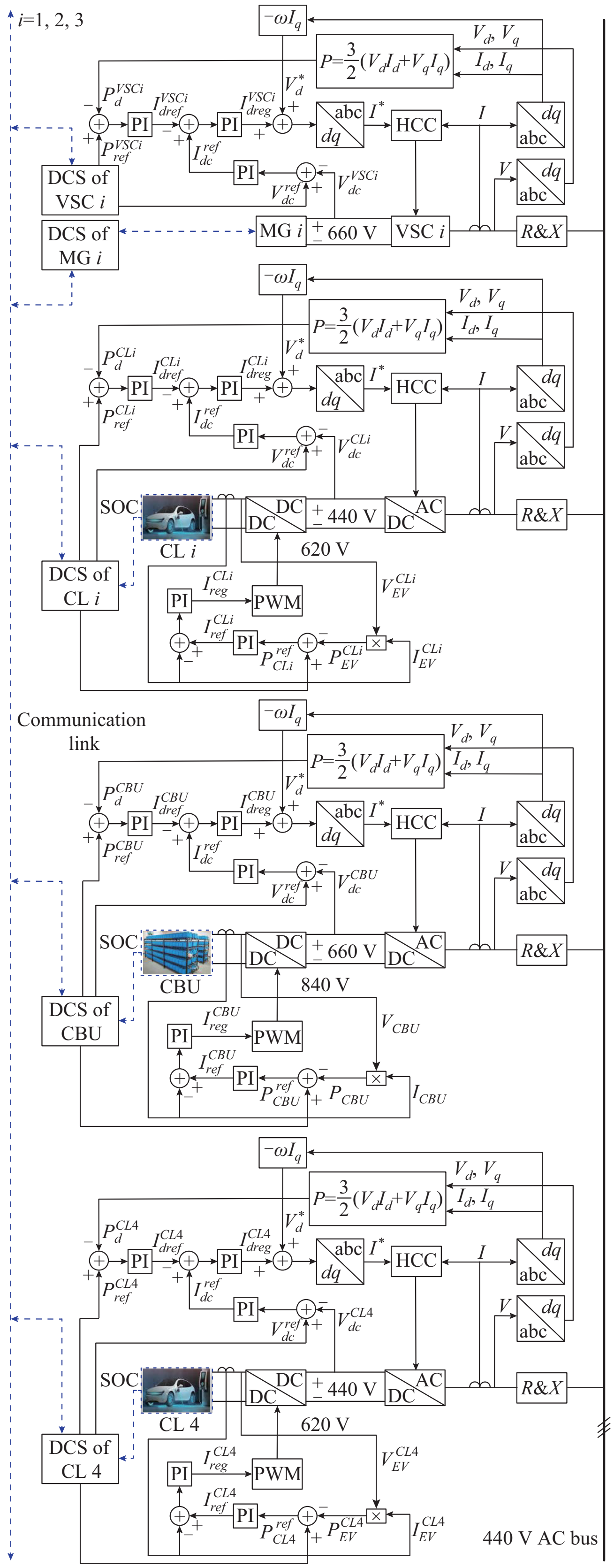

Fig. 4. DCS for implementing proposed DPMSs of off-grid DCFC-MMG.

After activating the AC-DC converters in MGs 1-3, CLs 1-4, and the CBU, the DC-DC converters on the CL side are triggered to charge EVs 1-4 at 620 V/150 kW. The purpose for selecting a constant-power EV charging is provided in Supplementary Material A.

$$\boldsymbol{T}_{\mathrm{abc}}^{dq}=\begin{bmatrix}\cos(\omega t) & -\sin(\omega t)\\ \cos(\omega t-2\pi/3) & -\sin(\omega t-2\pi/3)\\ \cos(\omega t+2\pi/3) & -\sin(\omega t+2\pi/3)\end{bmatrix} \quad (7)$$

$$\begin{cases} I_{\mathrm{a}}^{VSCj}=I_{\mathrm{a}}^{*}-I_{\mathrm{a}}\\ I_{\mathrm{b}}^{VSCj}=I_{\mathrm{b}}^{*}-I_{\mathrm{b}}\\ I_{\mathrm{c}}^{VSCj}=I_{\mathrm{c}}^{*}-I_{\mathrm{c}}\end{cases} \quad (8)$$

For CL i, the charging power P_{EV}^{CLi} calculated in (9) is compared with the reference power specified by the corresponding DCS of CL. This comparison is used to calculate the reference and regulated currents using two PI controllers. The resulting current is then applied to the PWM converter to generate the required gating signals for the DC-DC converter. Additionally, the DC-DC converter of the CBU can be activated either to supply power for charging EV 4 located at CL 4 or to absorb power from MGs 1-3 when their corresponding CLs are unoccupied.

$$P_{EV}^{CLi}=V_{EV}^{CLi}I_{EV}^{CLi} \quad (9)$$

where V_{EV}^{CLi} and I_{EV}^{CLi} are the required charging voltage and current for CL i, respectively.

The PI controller gain parameters for the control loops and the filter tuning coefficients are listed in Supplementary Material A Tables SAI and SAII, respectively. The control system complexities are summarized in Table SAIII.

B. MG2MG Operation in MGs 1-3 Under Battery Outage Conditions

To implement DPMSs among MGs, if the battery in any MG is disconnected from the circuit, the other MGs take over the internal three-phase load of the MG that has experienced an outage. Meanwhile, the CBU, in addition to charging EV 4, takes over the charging power of the EV previously supplied by the affected MG. Therefore, MGs 1-3 can continue to operate, and CLs 1-4 remain powered.

As illustrated in Fig. 5(a), under battery outage conditions in MG 1, MGs 2 and 3 deliver power to MG 1 through BCs 1 and 3, respectively, and the proposed DPMSs ensure the uninterrupted operation of MG 1. In MG 1, when the battery is disconnected from the circuit, the communication link enables coordination among the DCS of MGs 1-3, the DCS of BCs 1-3, and the DCS of CBU. This coordination ensures that the power required to supply the load of MG 1 is equally shared between MGs 2 and 3. Meanwhile, EVs 2 and 3 are charged by MGs 2 and 3, respectively, whereas EVs 1 and 4 are charged by the CBU. Consequently, the load power of MG 1 is supplied by MGs 2 and 3, while the charging power for EV 1, which is supplied by MG 1 under normal conditions, is transferred to the CBU under critical conditions. To activate BC 1 and facilitate the power transfer from MG 2 to MG 1, half of the load power of MG 1 P_{L}^{MG1}, which has already been transformed into the d-axis using (3), is divided by half of the DC link voltage of MG 2 to generate the reference current, as described in (10). This reference current is then compared with the current injected by BC 1 into MG 1. The resulting error is processed through a

PI controller to obtain a regulated current, which is converted into appropriate PWM pulses to trigger BC 1. A similar procedure is followed to activate BC 3 for power transfer from MG 3 to MG 1. It is worth noting that (10) is applicable only when the battery of one MG is disconnected from the circuit and that MG requires auxiliary power from the other two MGs. Accordingly, each healthy MG supplies half of the load power of the failed MG. If a battery outage occurs in MG 2 or MG 3, an analogous process is executed, as illustrated in Fig. 5(b) and (c), respectively. Additional explanation for Fig. 5 is provided in Supplementary Material A.

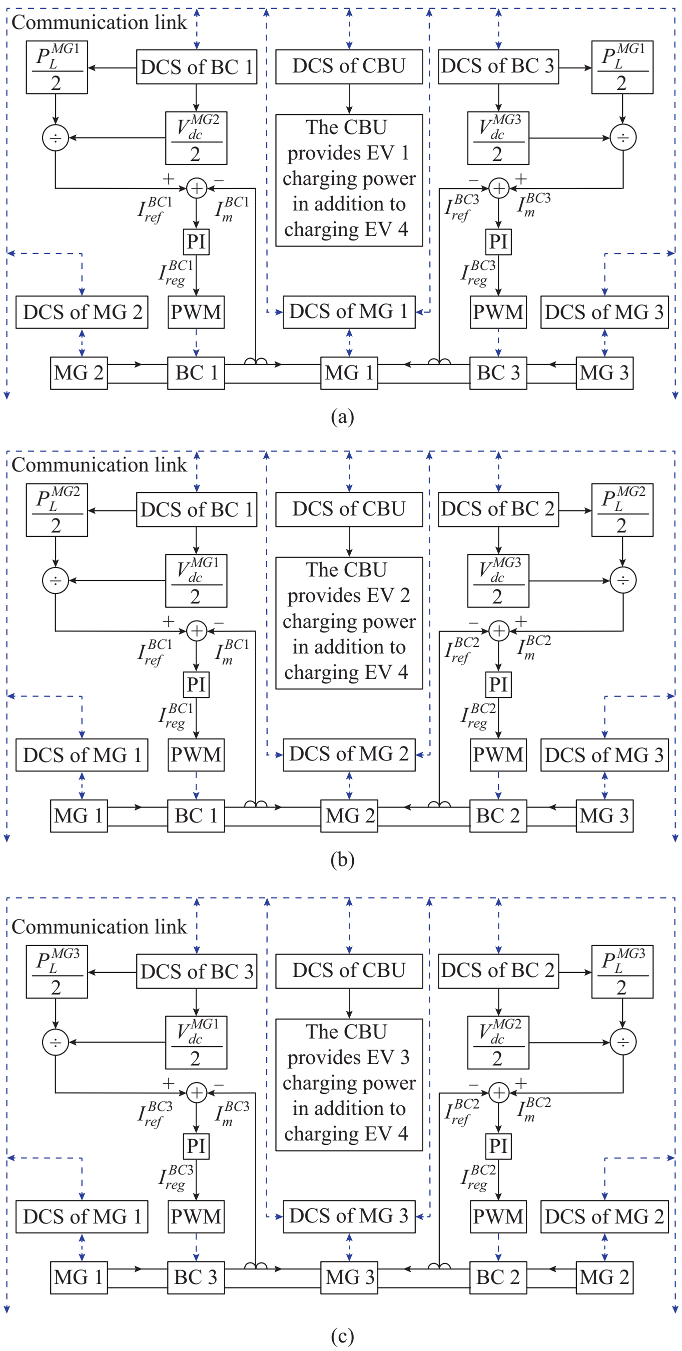

Fig. 5. Proposed DPMSs for case in which MGs mutually support each other to ensure uninterrupted operation under battery outage conditions. (a) Under battery outage conditions in MG 1. (b) Under battery outage conditions in MG 2. (c) Under battery outage conditions in MG 3.

$$I_{ref}^{i}=\frac{P_L^{MG1}}{2}\Bigg/\left(\frac{V_{dc}^{j}}{2}\right)\quad i=1,3,\ j=2,3 \tag{10}$$

C. V2V and V2MG Operation Under Simultaneous Battery Outage Conditions in MGs 1-3

Under simultaneous battery outage conditions in MGs 1-3, the proposed DPMSs operate as shown in the flowchart in Fig. 6, where the V2V and V2MG capabilities are activated according to the outage conditions.

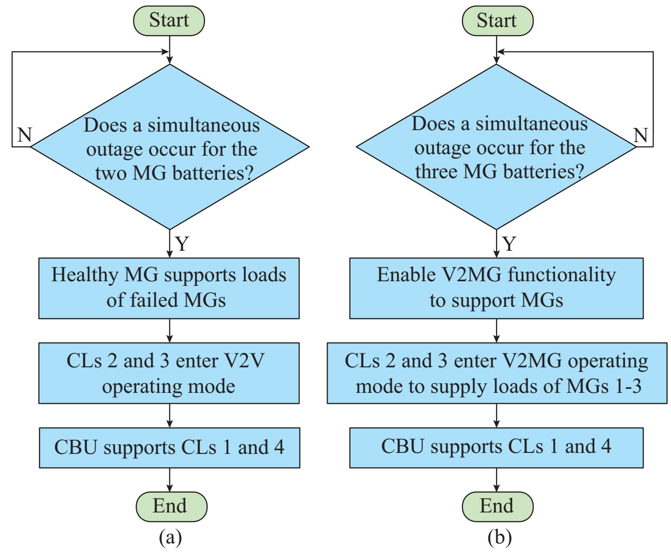

Fig. 6. Flowchart of proposed DPMSs for activating V2V and V2MG capabilities under simultaneous battery outage conditions in MGs 1-3. (a) V2V. (b) V2MG.

If the batteries of two MGs are out of circuit simultaneously, the healthy MG, in addition to supplying its own load, also takes on the load of the failed MGs and no longer shares power to charge the CLs. In this case, CLs 2 and 3 enter the V2V operating mode, such that one of them is charged by the other. Meanwhile, CLs 1 and 4 are supplied by the CBU. Therefore, the loads of all three MGs are supplied, while three EVs operate in charging mode and one EV operates in discharging mode.

If the batteries of all three MGs are out of the circuit simultaneously, the V2MG capability is activated so that CLs 2 and 3, which were previously under charging, operate in discharging mode to supply power to MGs 1-3. The CBU also provides charging power for CLs 1 and 4. Therefore, the loads of the three MGs are supplied by CLs 2 and 3, while two EVs are charged by the CBU.

D. MGs Operating in Off-grid Mode

Figure 7 illustrates the proposed DPMSs for each MG operating in off-grid mode using DCS. The DCS is responsible for monitoring and managing the battery, load, and PV units to stabilize the DC bus voltage by balancing power generation and consumption. It should be noted that the PV unit is designed to inject the maximum available power into the DC bus to maintain the reference voltage [32]. However, due to the inherent uncertainty in PV generation, which may lead to voltage fluctuations under variable load conditions, the battery provides supplementary support to ensure the voltage stability.

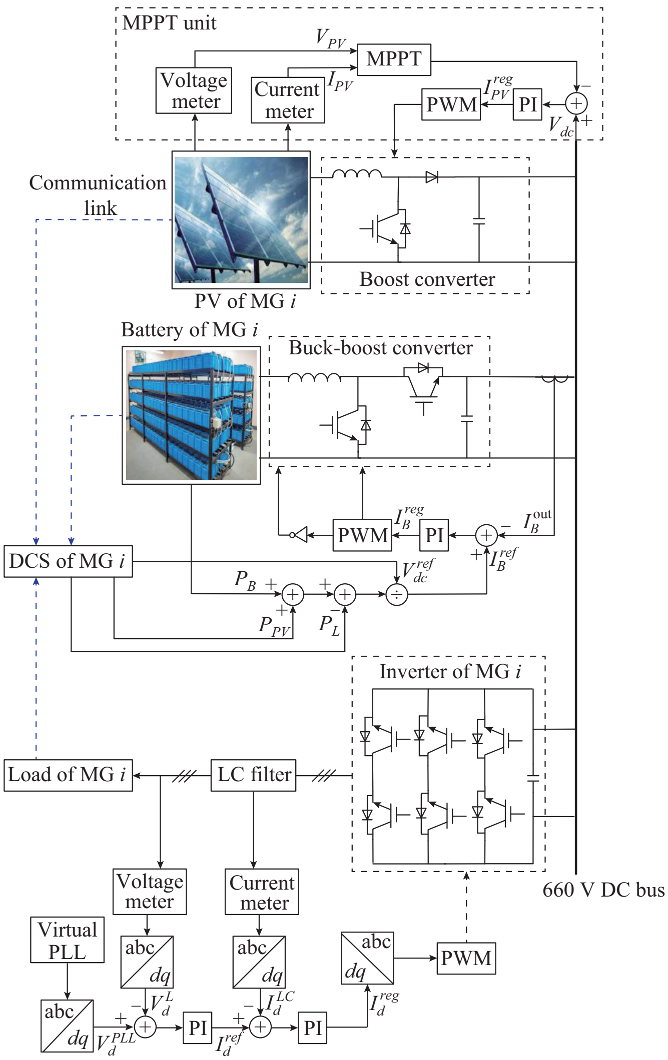

Fig. 7. Proposed DPMSs for each MG operating in off-grid mode using DCS.

The average model of a boost converter with a PV unit connected at the input side is derived in (11), and the output power of the PV unit P_{PV} is calculated in (12).

$$\begin{cases} L_{bo}\dfrac{\mathrm{d}I_{PV}}{\mathrm{d}t}=V_{PV}-(1-D)V_{dc} \\ C_{dc}\dfrac{\mathrm{d}V_{dc}}{\mathrm{d}t}=(1-D)I_{PV}-\dfrac{P_{PV}}{V_{dc}} \end{cases} \tag{11}$$

$$P_{PV}=I_{PV}V_{PV} \tag{12}$$

where L_{bo} is the inductance of the boost converter; C_{dc} is the DC link capacitor; V_{PV} is the voltage of the PV unit; I_{PV} is the current of the PV unit; and D is the duty cycle of the PWM converter.

Bu using a PI controller, the regulated current is obtained, which is then used to compute the appropriate PWM duty cycle for activating the boost converter. To feed the load, the inverter employs a switching strategy based on a virtual phase-locked loop (PLL). This system generates a reference voltage at the desired frequency [33]. This reference voltage is compared with the load voltage, both expressed on the d-axis. The resulting error generates a reference current, which is subsequently compared with the three-phase current passing through the LC filter and transformed into the d-axis. Finally, this current is converted back to the three-phase domain, and appropriate PWM pulses are generated to trigger the load-side inverter. To manage the battery, the DCS first calculates the power of battery P_B using (13). The net power is divided by the reference voltage of the DC bus to determine the battery reference current, as expressed in (14). P_B is added to the output power of the PV unit, and the total load demand is subtracted from the resulting sum. By comparing this reference current with the output current of the battery converter, a regulated current can be obtained. This regulated current is subsequently used to generate suitable PWM pulses for charging or discharging the battery through the buck-boost converter.

$$P_B=V_BI_B \tag{13}$$

$$I_B^{ref}=\frac{P_{PV}+P_B-P_L}{V_{dc}^{ref}} \tag{14}$$

where V_B and I_B are the voltage and current of the battery, respectively.

IV. Numerical Results

A. Performance of Off-grid DCFC-MMG Under MMG Uncertainty and CBU Outage Conditions

Figure 8 shows the charging power delivered to CLs 1-4. where four EVs parked in CLs 1-4 are charged at 0.1, 0.15, 0.2, and 0.25 s, respectively. The charging process is completed in 0.7 s for EVs 1 and 2, and in 0.75 s for EVs 3 and 4.

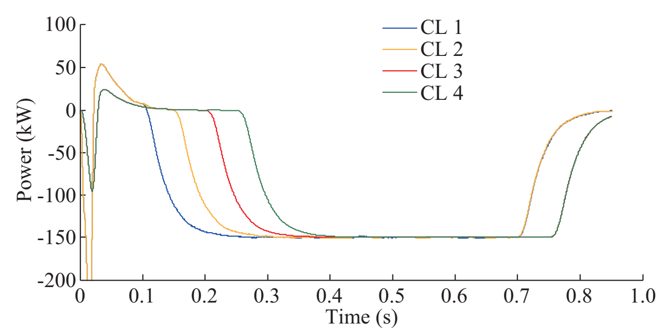

Fig. 8. Charging power delivered to CLs 1-4.

The charging power delivered to CLs 1-4 is supplied by MGs 1-3 and the CBU, as shown in Fig. 9, where the power injection process from MGs 1-3 and the CBU (each 150 kW) is activated at 0.1, 0.15, 0.2 and 0.25 s to charge EVs 1-4, respectively. When the CBU disconnects at 0.35 s, MGs 1-3 increase their outputs by 50 kW to provide charging power for EV 4. However, at 0.45 s, as the PV power generation of MG 1 (according to Fig. 10) falls below 0.3 p.u., the DCS prevents it from supporting the CBU. MGs 2 and 3 then compensate by supplying the additional required power.

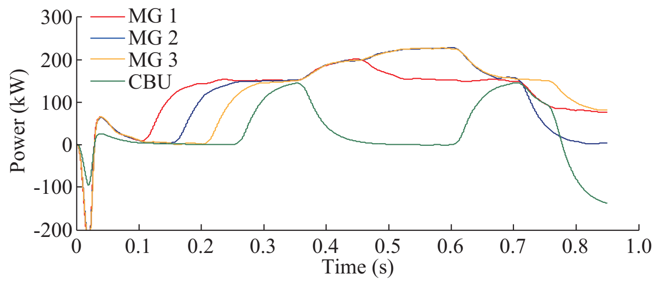

Fig. 9. Power of MGs 1-3 and CBU to deliver charging power for CLs 1-4.

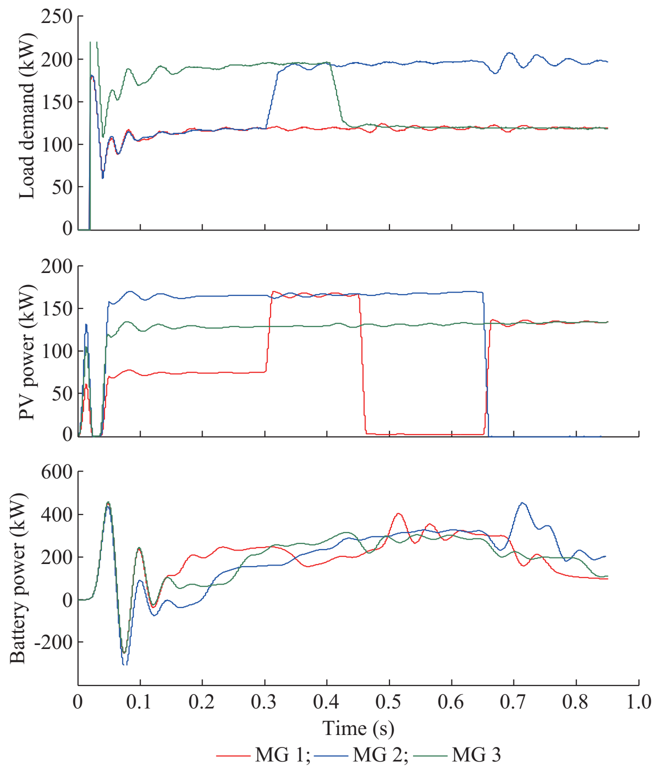

Fig. 10. Uncertainties of load demands, PV power, and battery power of MGs 1-3.

As a result, the output power of MG 1 returns to 150 kW, while both MGs 2 and 3 operate at 225 kW. At 0.6 s, when the CBU returns to operation, the power of MGs 2 and 3 decreases from 225 kW to 150 kW, returning to the pre-outage conditions. At 0.7 s, the power of MG 1 decreases from 150 kW to 75 kW as it completes charging EV 1, allowing MG 1 to charge the CBU at 75 kW. In MG 2, PV power generation becomes zero at 0.65 s. Therefore, when EV 2 completes charging at 0.7 s, MG 2 does not supply power to the CBU. At 0.75 s, after EVs 3 and 4 have completed charging, MG 3 contributes 75 kW power to the CBU. In total, the CBU receives 150 kW power (75 kW from MG 1 and 75 kW from MG 3). Thus, MGs 1-3 are able to charge EVs 1-4 in both the presence and absence of the CBU, support the CBU, and charge it at empty CLs. Moreover, according to Fig. 10, they properly supply their internal loads considering generation uncertainty and demand fluctuations.

Figure 11 also shows the three-phase currents of VSCs of CLs 1-4, MGs 1-3, and CBU. As observed, variations in the three-phase currents of VSCs of MGs 1-3 and CBU, which are proportional to the power conditions of Fig. 9, do not negatively affect the three-phase currents of AC-DC converters of CLs 1-4, which are proportional to the power conditions of Fig. 8. The currents of these CLs remain completely uniform during the EV charging process.

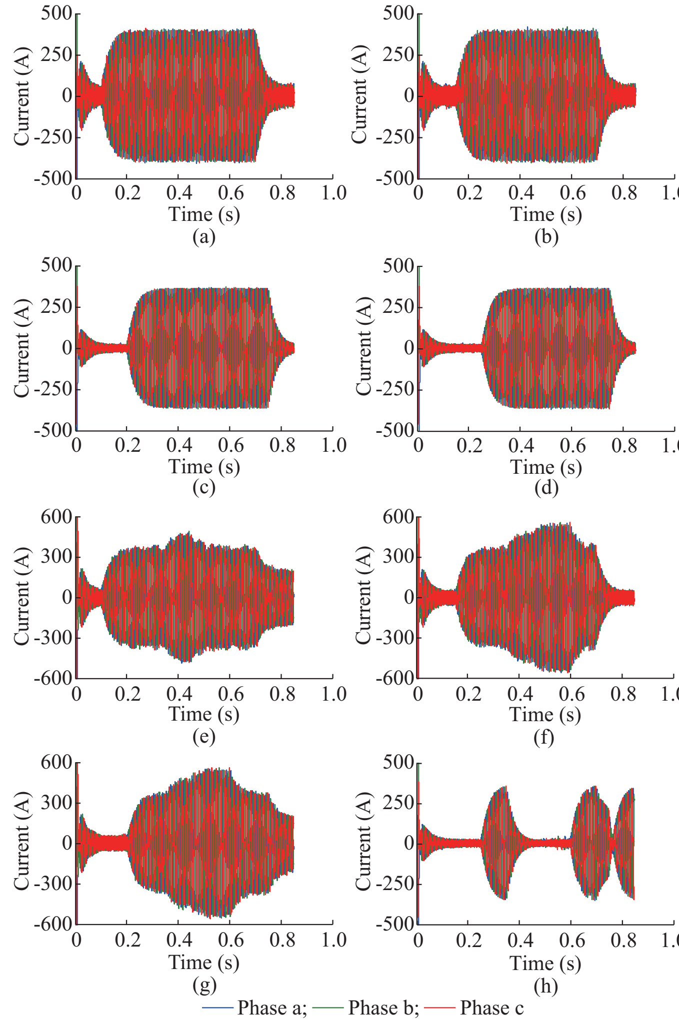

Fig. 11. Three-phase currents of VSCs of CLs 1-4, MGs 1-3, and CBU. (a) CL 1. (b) CL 2. (c) CL 3. (d) CL 4. (e) MG 1. (f) MG 2. (g) MG 3. (h) CBU.

Considering the start and end time of the charging process of CLs 1-4 according to the conditions of Fig. 8, Fig. 12 displays the charging power of CLs 1-4 supplied by MGs 1-3 and CBU when the control and management schemes of [11], [14], [20], and [22] are applied instead of the proposed DPMSs in this paper, under uncertainty and outage conditions from 0.35 to 0.6 s. Each of MGs 1-3 and CBU successfully injects 150 kW power into CLs 1-4 at 0.1, 0.15, 0.2, and 0.25 s, respectively. However, during the CBU outage from 0.35 to 0.6 s, the absence of the proposed DPMSs under uncertainty and outage conditions results in CL 4 without power. Once the CBU is reconnected to the circuit at 0.6 s, its power is restored to charge CL 4. Additionally, when the charging process is completed, the power to all MGs and the CBU drops to zero, and the CBU is not charged. Additional explanations of Fig. 12 are provided in Supplementary Material A.

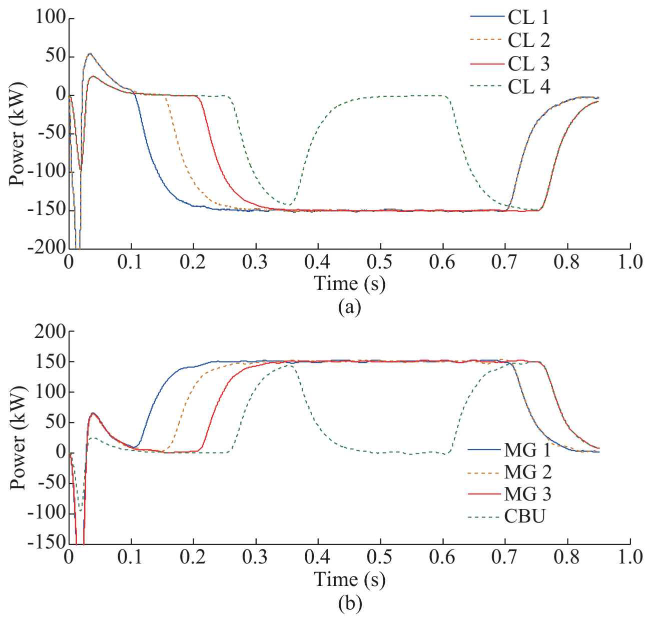

Fig. 12. Charging power of CLs 1-4 supplied by MGs 1-3 and CBU under operation of schemes in [11], [14], [20], and [22]. (a) CLs 1-4. (b) MGs 1-3 and CBU.

B. *Performance of Off-grid DCFC-MMG Under Battery Outage Conditions in MGs*

Figure 13 illustrates the power variations of the loads and batteries of MGs 1-3, assuming that EVs 1 and 4 are charged by MG 1 and CBU from 0.15 s, respectively, EV 2 is charged by MG 2 from 0.1 s, and EV 3 is charged by MG 3 from 0.2 s. In addition, the PV power generation in the MGs is assumed to be zero. The battery of MG 1 is then disconnected from the circuit from 0.25 to 0.45 s. Therefore, the proposed DPMSs should operate appropriately to achieve mutual support among MGs and provide charging power for EVs 1-4. However, when the battery of MG 1 is disconnected, according to Fig. 13, the load of MG 1 is supplied by the batteries of MGs 2 and 3. According to Fig. 14, the charging power of CL 1, which is supplied by MG 1 before the battery outage, is provided by the CBU. Therefore, from 0.25 s to 0.45 s, the output power of the CBU is 300 kW, and MGs 2 and 3 only provide charging power for CLs 2 and 3, and do not participate in charging CL 1, as they jointly supply the load of MG 1. From 0.25 to 0.45 s, the CBU provides the charging power required for both CL 1 and CL 4. After the battery of MG 1 is reconnected to the circuit at 0.45 s, the charging power in Fig. 14 decreases again to 150 kW for charging CL 4. The battery power of MGs 1-3 in Fig. 13 is proportional to their internal three-phase loads and the CLs under their supply. Figure 14(b) shows the three-phase current of VSC of the CBU, which corresponds to the power variations of the CBU.

Consequently, when the battery of MG 1 is disconnected, the CBU charges CLs 1 and 4 simultaneously. Meanwhile, MGs 2 and 3, in addition to charging CLs 2 and 3, supply their own loads and jointly support the load of MG 1.

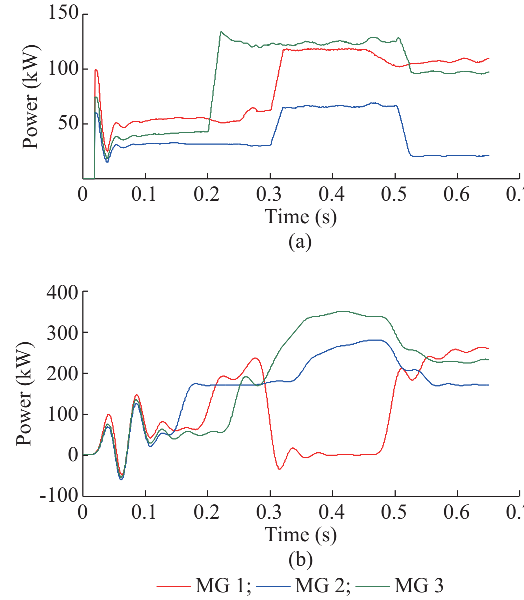

Fig. 13. Power variations of loads and batteries of MGs 1-3. (a) Loads. (b) Batteries.

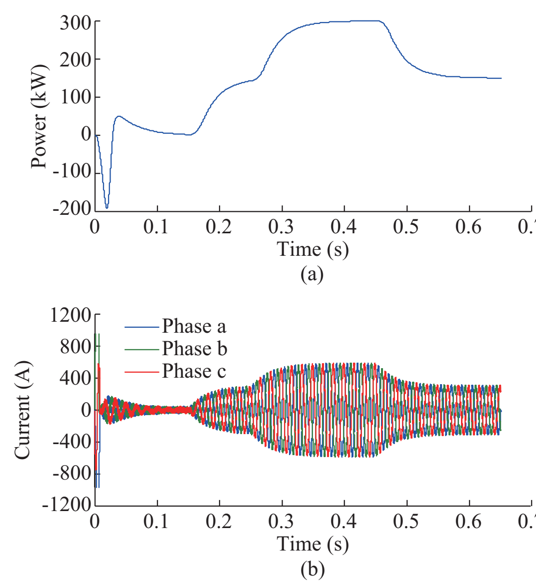

Fig. 14. Charging power and three-phase current of VSC of CBU. (a) Charging power. (b) Three-phase current.

The power of MGs 1-3 and CBU during the battery outage in MG 1 is presented in Table II before, during, and after the battery outage of MG 1, with values corresponding to Figs. 13 and 14.

In Fig. 15, the control and management schemes of [8], [9], [10], and [23] do not address the outage conditions occurring in one MG and receiving support from another MG, while considering the power requirements of the CLs. Therefore, when the battery of MG 1 is disconnected from the circuit, both the load power of MG 1 and the charging power of CL 1 (previously supplied by MG 1) remain unserved. Consequently, the power drops to zero from 0.25 s to 0.45 s. After the battery of MG 1 is reconnected, the load and charging power are restored. Therefore, compared with the proposed DPMSs in this paper, which, during the battery outage in MG 1, supplies the load power of MG 1 through MGs 2 and 3 and provides the charging power of CL 1 through the CBU, the schemes of the above-mentioned references can neither supply the load of MG 1 nor charge CL 1.

TABLE II
POWER OF MGS 1-3 AND CBU DURING BATTERY OUTAGE IN MG 1

Time (s)	Power of MG 1 (kW)			Power of MG 2 (kW)				Power of MG 3 (kW)				Power of CBU (kW)	
	Load	Battery	Injected into CL 1	Load	Battery	Injected into CL 2	Injected into MG 1	Load	Battery	Injected into CL 3	Injected into MG 1	Injected into CL 1	Injected into CL 4
0.10	50	52	0	25	28	0	0	40	42	0	0	0	0
0.25	49	200	150	25	178	150	0	40	192	150	0	0	150
0.45	120	0	0	60	275	150	60	130	345	150	60	150	150
0.65	110	265	150	20	175	150	0	95	245	150	0	0	150

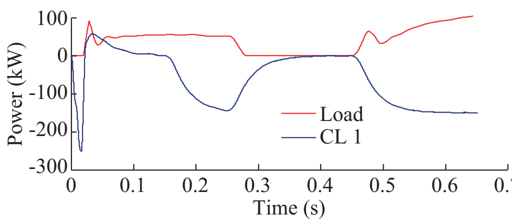

Fig. 15. Load power of MG 1 and CL 1 under operation of schemes of [8], [9], [10], and [23].

C. Performance of Off-grid DCFC-MMG Under Simultaneously Battery Outage Conditions in MGs

Figure 16 illustrates the power variations of batteries in MGs 1-3, assuming that the charging conditions for CLs and the load conditions for MGs are the same as those described previously. In addition to the battery of MG 1, the battery of MG 2 also experiences an outage from 0.25 to 0.45 s, and is removed from the circuit. Therefore, the battery of MG 3 supplies the load of all three MGs and its output power increases to approximately 300 kW.

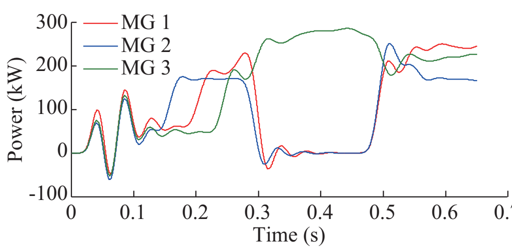

Fig. 16. Power variations of batteries in MGs 1-3.

Figure 17 shows the power variations of CLs 2 and 3 under V2V operation and under simultaneous battery outage conditions in MGs 1 and 2. Before the outages in MGs 1 and 2, both CLs are operating in charging mode. During the outages, CL 3 switches to discharging mode and supplies power to charge CL 2. After the outages end, both CLs return to charging mode and resume the normal operation. CLs 1 and 4 are also charged by the CBU, as shown in Fig. 14.

If the battery of MG 3 is also disconnected from 0.25 s to 0.45 s in Fig. 16, the power variations of CLs 1-4 are shown in Fig. 18. During this period, CLs 1 and 4 are charged by the CBU, while CLs 2 and 3 operate in discharging mode and provide load power to MGs 1 to 3 through V2MG operation.

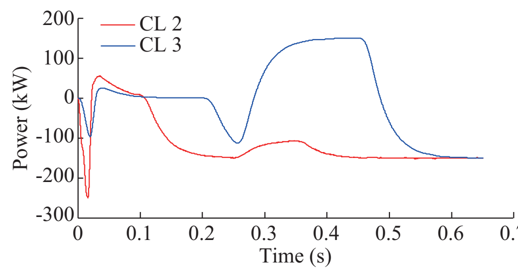

Fig. 17. Power variations of CLs 2 and 3 under V2V operation and under simultaneous battery outage conditions in MGs 1 and 2.

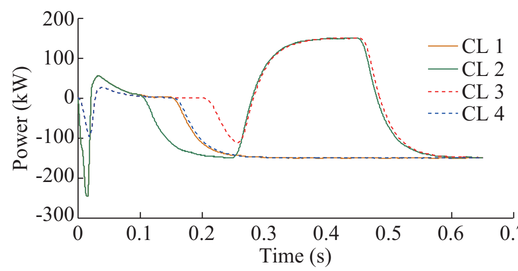

Fig. 18. Power variations of CLs 1-4 under simultaneous battery outage conditions in MGs 1-3.

D. Performance of Off-grid MGs While Supporting Each Other

In this subsection, the performance of MG 2 is analyzed. It is demonstrated that while the MGs support each other and inject power into the CLs, the internal operating conditions of the MGs are normal and their loads are properly supplied. Therefore, Fig. 19 illustrates the three-phase load voltage and current of MG 2 under the load power conditions in Fig. 13.

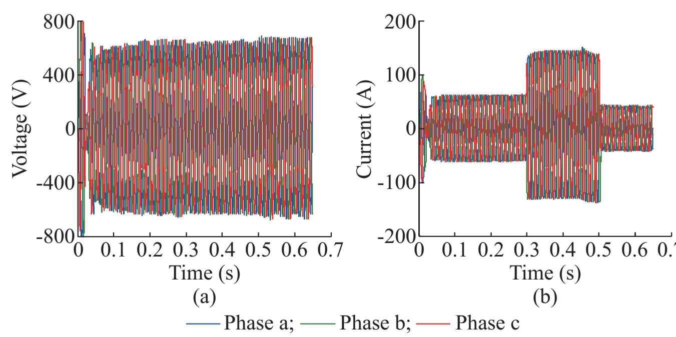

Fig. 19. Three-phase load voltage and current of MG 2 under load power conditions in Fig. 13. (a) Voltage. (b) Current.

Following the load power variations of MG 2 in Fig. 13, the load current also varies in Fig. 19. Nevertheless, the load voltage remains stable within the acceptable operating range.

Figure 20 shows the DC link voltage and generated frequency of load inverter in MG 2, where the frequency variations under different operating conditions are less than 0.1 Hz. The DC link voltage stabilizes at 660 V after transient disturbances. According to Fig. 13, at 0.25 s, MG 2 assists MG 1, which causes the DC link voltage of MG 2 to drop to 650 V. At 0.3 s, as the load of MG 2 increases, the DC link voltage of MG 2 decreases further to 640 V, but it quickly returns to the nominal value due to the operation of the DCS. At 0.45 s, when the battery of MG 1 is reconnected and MG 2 is no longer required to support MG 1, the load previously transferred to MG 2 is returned to MG 1, resulting in a sudden increase in the DC link voltage of MG 2. The control system stabilizes the voltage. However, as the internal load of MG 2 decreases at 0.5 s, another temporary increase in DC link voltage occurs, which is again corrected by the DCS, and the voltage stabilizes at 660 V from 0.52 s onward.

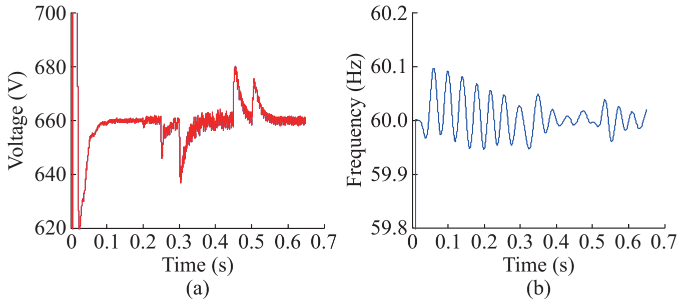

Fig. 20. DC link voltage and generated frequency of load inverter in MG 2. (a) DC link voltage. (b) Frequency.

Since the voltage control systems used in [12], [13], [19], and [24] are not designed for conditions where two MGs are interconnected for power exchange while considering outages of storage units, the results shown in Fig. 21 are obtained when these schemes are applied to the off-grid DCFC-MMG under study. As illustrated, when MG 2 is connected to MG 1 for power injection between 0.25 and 0.45 s, significant oscillations occur in the DC link voltage of MG 2. Moreover, after 0.45 s, when the MGs are disconnected, the DC link voltage does not stabilize at its nominal value. These oscillations in the DC link voltage lead to fluctuations in the three-phase voltage of the load inverter in MG 2, resulting in a non-standard voltage supply to the load. Therefore, the voltage control system under interconnected MG operation, especially when one MG experiences the outage of a storage unit, is handled more effectively by the proposed DPMSs than other schemes. A quantitative comparison of the results shown in Figs. 20 and 21 is provided in Supplementary Material A.

Finally, it should be noted that a comprehensive economic analysis demonstrating the superiority of the proposed DPMSs over the baseline scheme is described in Supplementary Material A. Compliance with operational implementation standards and future research directions are also outlined in Supplementary Material A.

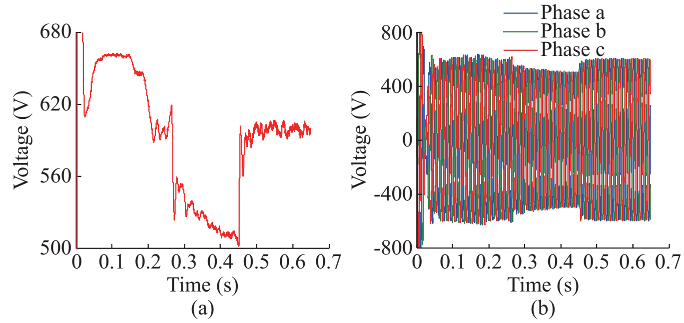

Fig. 21. DC link voltage and three-phase load voltage in MG 2 under operation of schemes in [12], [13], [19], and [24]. (a) DC link voltage. (b) Three-phase load voltage.

V. Conclusion

The proposed DPMSs in this paper using DCSs ensure the reliable operation of an off-grid DCFC-MMG under uncertainty and outage conditions. The results demonstrate that the internal loads of all MGs are properly supplied, the charging power of all CLs is continuously delivered, and effective mutual support among MGs and to the CBU is achieved under uncertainty and outage conditions.

Under normal operation with the CBU in service, MGs 1-3 supply the charging power of CLs 1-3, respectively, while the CBU is responsible for supplying CL 4. After the completion of the EV charging process, each MG, considering the generation uncertainty, contributes to charging the CBU with half of the nominal charging power.

Under CBU outage conditions, MGs 1-3 collectively supply the charging power required by EV 4, while considering generation uncertainty. In this mode, only MGs with PV generation exceeding 0.3 p.u. participate in sharing the charging power.

Under battery outage conditions in any MG, the remaining MGs provide necessary support to supply the internal load of the affected MG. Simultaneously, the charging power previously assigned to the failed MG is transferred to the CBU, ensuring uninterrupted operation of the DCFC station.

Across all the aforementioned operating conditions, the three-phase loads of MGs remain well-supplied. Neither demand fluctuations, generation uncertainty, power sharing among MGs under different charging conditions, nor mutual support during outage events result in undesirable fluctuations in voltage, current, or frequency.

Overall, the proposed DPMSs in this paper successfully maintain the charging operation of CLs 1-4 under both normal and critical conditions, enabling effective power exchange among MGs while preserving acceptable electrical performance even during battery outages. Furthermore, by implementing V2V and V2MG capabilities, the off-grid DCFC-MMG sustains continuous operation under simultaneous battery outage conditions in MGs.

References

[1] G. Rituraj, G. R. C. Mouli, and P. Bauer, "A comprehensive review on off-grid and hybrid charging systems for electric vehicles," *IEEE Open Journal of the Industrial Electronics Society*, vol. 3, pp. 203-222, Apr. 2022.

[2] T. Yuvaraj, K. R. Devabalaji, J. A. Kumar *et al.*, "A comprehensive review and analysis of the allocation of electric vehicle charging stations in distribution networks," *IEEE Access*, vol. 12, pp. 5404-5461, Jan. 2024.

[3] Y. Wu, Z. Wang, Y. Huangfu *et al.*, "Hierarchical operation of electric vehicle charging station in smart grid integration applications – an overview," *International Journal of Electrical Power & Energy Systems*, vol. 139, p. 108005, Jul. 2022.

[4] G. Arena, A. Chub, M. Lukianov *et al.*, "A comprehensive review on DC fast charging stations for electric vehicles: standards, power conversion technologies, architectures, energy management, and cybersecurity," *IEEE Open Journal of Power Electronics*, vol. 5, pp. 1573-1611, Sept. 2024.

[5] J. Suvvala, S. K. Sathish, C. Dhananjayulu *et al.*, "Integration of renewable energy sources using multiport converters for ultra-fast charging stations for electric vehicles: an overview," *Heliyon*, vol. 10, p. e35782, Aug. 2024.

[6] X. Liu, T. Zhao, H. Deng *et al.*, "Microgrid energy management with energy storage systems: a review," *CSEE Journal of Power and Energy Systems*, vol. 9, no. 2, pp. 483-504, Mar. 2023.

[7] J. Sarda, N. Patel, H. Patel *et al.*, "A review of the electric vehicle charging technology, impact on grid integration, policy consequences, challenges and future trends," *Energy Reports*, vol. 12, pp. 5671-5692, Jan. 2024.

[8] M. Asna, H. Shareef, A. Prasanthi *et al.*, "A novel multi-level charging strategy for electric vehicles to enhance customer charging experience and station utilization," *IEEE Transactions on Intelligent Transportation Systems*, vol. 25, no. 9, pp. 11497-11508, Mar. 2024.

[9] D. Cui, Z. Wang, P. Liu *et al.*, "Coordinated charging scheme for electric vehicle fast-charging station with demand-based priority," *IEEE Transactions on Transportation Electrification*, vol. 10, no. 3, pp. 6449-6459, Nov. 2023.

[10] H. T. Nguyen and D. H. Choi, "Distributionally robust model predictive control for smart electric vehicle charging station with V2G/V2V capability," *IEEE Transactions on Smart Grid*, vol. 14, no. 6, pp. 4621-4633, Mar. 2023.

[11] H. Arya and M. Das, "Fast charging station for electric vehicles based on DC microgrid," *IEEE Journal of Emerging and Selected Topics in Industrial Electronics*, vol. 4, no. 4, pp. 1204-1212, Jun. 2023.

[12] D. Yan, J. Zhu, F. Liu *et al.*, "A nested distributed coordination mechanism for charging stations with shared energy storage," *CSEE Journal of Power and Energy Systems*, vol. 9, no. 5, pp. 1-12, Sept. 2023.

[13] M. Dicorato, G. Forte, F. Marasciuolo *et al.*, "Integration of EV fast charging station into a DC-based microgrid," *IEEE Transactions on Industry Applications*, vol. 61, no. 3, pp. 1-11, Feb. 2025.

[14] D. Zhang, W. Fu, J. Qin *et al.*, "Robust cooperative operation of community microgrids with electric vehicle battery charging stations and swapping stations," *IEEE Transactions on Industrial Informatics*, vol. 21, no. 5, pp. 1-11, Apr. 2025.

[15] N. Poursafar, S. Taghizadeh, M. J. Hossain *et al.*, "A voltage-supportive controller for ultra-fast electric vehicle chargers in islanded DC microgrids," *Journal of Modern Power Systems and Clean Energy*, vol. 11, no. 3, pp. 896-906, May 2023.

[16] K. Li, C. Shao, X. Huang *et al.*, "Day-ahead charging capacity market for power distribution network with electric vehicle charging stations," *IEEE Transactions on Power Systems*, vol. 40, no. 3, pp. 2258-2271, May 2025.

[17] H. Li, M. A. Azzouz, and A. A. Hamad, "Cooperative voltage control in MV distribution networks with electric vehicle charging stations and photovoltaic DGs," *IEEE Systems Journal*, vol. 15, no. 2, pp. 2989-3000, Jun. 2021.

[18] B. K. Saw and A. K. Bohre, "Sustainable deployment of EV charging stations in distribution network supported with hybrid solar-DG integrated DSTACOM," *IEEE Transactions on Industry Applications*, vol. 61, no. 3, pp. 1-16, Feb. 2025.

[19] K. Tiwari and B. Singh, "Control framework to deal operational challenges in RES-based distribution network powering EV charging station," *IEEE Transactions on Transportation Electrification*, vol. 11, no. 1, pp. 1015-1025, May 2025.

[20] M. Khalid and B. K. Panigrahi, "Decentralized power management in multi BESS-PV based charging infrastructure for EV with SoC balancing," *IEEE Transactions on Industry Applications*, vol. 59, no. 6, pp. 7392-7403, Aug. 2023.

[21] A. Abuelrub, F. Hamed, J. Hedel *et al.*, "Feasibility study for electric vehicle usage in a microgrid integrated with renewable energy," *IEEE Transactions on Transportation Electrification*, vol. 9, no. 3, pp. 4306-4315, Feb. 2023.

[22] B. Tan, Z. Lin, X. Zheng *et al.*, "Distributionally robust energy management for multi-microgrids with grid-interactive EVs considering the multi-period coupling effect of user behaviors," *Applied Energy*, vol. 350, p. 121770, Nov. 2023.

[23] H. Faraji, G. B. Gharehpetian, A. Khorsandi *et al.*, "Multiple control strategies for distributed battery energy storages in microgrid DC fast charging stations to improve load voltage variations, mutual power exchange with the grid and islanded mode operation," *IEEE Transactions on Transportation Electrification*, vol. 10, no. 4, pp. 10388-10400, Dec. 2024.

[24] K. El Mezdi, A. El Magri, and L. Bahatti, "Advanced control and energy management algorithm for a multi-source microgrid incorporating renewable energy and electric vehicle integration," *Results in Engineering*, vol. 23, p. 102642, Sept. 2024.

[25] A. Elsanabary, K. Khairullah, N. F. A. Aziz *et al.*, "Power management and optimized control of hybrid PV-BESS-grid integrated fast EV charging stations," *Journal of Energy Storage*, vol. 90, p. 111802, Jun. 2024.

[26] U. K. Kundu, M. Singh, A. Giri *et al.*, "Robust and fast control approach for islanded microgrid system and EV charging station applications," *Electrical Engineering*, vol. 107, pp. 8385-8396, Mar. 2024.

[27] M. Sadiq, C. Su, Z. Ali *et al.*, "Decentralized model predictive control for offshore wind-powered seaport DC microgrids with electric vehicle stations," *IEEE Transactions on Industry Applications*, vol. 61, no. 2, pp. 2258-2270, Jan. 2025.

[28] P. Harsh and D. Das, "A multi-objective energy scheduling of the reconfigurable off-grid microgrid with electric vehicles using demand response program," *Computers and Electrical Engineering*, vol. 117, p. 109275, Jul. 2024.

[29] M. Junayed, A. Ahmed, N. K. Roy *et al.*, "A sustainable off-grid electric vehicle charging model using distributed energy resources for remote hill regions in Bangladesh," *Energy Conversion and Management*, vol. 348, p. 120519, Jan. 2026.

[30] M. Kumar, M. A. Shaikh, A. M. Soomro *et al.*, "Techno-economic comparative analysis of an off-grid PV-wind-hydrogen based EV charging station under four climatically distinct cities in Pakistan," *International Journal of Hydrogen Energy*, vol. 93, pp. 1268-1282, Dec. 2024.

[31] R. D. Kordkandi, M. T. Hagh, and S. Roozbehani, "Real-time low/high-voltage ride-through capability improvement of micro-grid based on coordinated robust grid-following control," *IET Generation, Transmission & Distribution*, vol. 16, no. 15, pp. 3045-3060, Jun. 2022.

[32] H. Faraji, A. Khorsandi, and S. H. Hosseinian, "Multi-level coordinated control of islanded DC microgrid integrated with electric vehicle charging stations with fault ride-through capability," *Journal of Cleaner Production*, vol. 420, p. 138372, Sept. 2023.

[33] M. Karimi-Ghartemani, M. Mojiri, A. Safaee *et al.*, "A new phase-locked loop system for three-phase applications," *IEEE Transactions on Power Electronics*, vol. 28, no. 3, pp. 1208-1218, Mar. 2013.

Hossien Faraji received the M.Sc. degree in electrical power engineering from Kermanshah University of Technology, Kermanshah, Iran, in 2020. He is currently pursuing the Ph.D. degree with Amirkabir University of Technology, Tehran, Iran. His research interests include control of microgrid and distributed generator, flexible alternating current transmission system (FACTS) device, high-voltage direct current (HVDC) system, and modeling and control of electric vehicle charging station and electric power system.

Amir Khorsandi received the B.Sc. and M.Sc. degrees in electrical engineering from Amirkabir University of Technology, Tehran, Iran, in 2008 and 2010, respectively, and the Ph.D. degree in electrical engineering from Sharif University of Technology, Tehran, Iran, in 2015. He is currently an Assistant Professor with Amirkabir University of Technology. His research interests include power quality, microgrid control, and application of power electronics in power distribution system.

Seyed Hossein Hosseinian received the Ph.D. degree in electrical engineering from University of Newcastle, Newcastle upon Tyne, U.K., in 1995. He is currently a Professor with the Department of Electrical Engineering, Amirkabir University of Technology, Tehran, Iran. His research interests include transient analysis of power system, power quality, restructuring, and deregulation of power system.